This is a repository copy of *The effect of alkyl chain length on the level of capping of silicon nanoparticles produced by a one-pot synthesis route based on the chemical reduction of micelle*.

Article:

The effect of alkyl chain length on the level of capping of silicon nanoparticles produced by a one-pot synthesis route based on the chemical reduction of micelle

Shane P. Ashby[1], Jason A. Thomas[1], Paul R. Coxon[1], Matthew Bilton[2], Rik Brydson[2], Timothy J. Pennycook[3,4] and Yimin Chao*[1]

[1] Energy Materials Laboratory, School of Chemistry, University of East Anglia, Norwich, NR4 7TJ, UK

[2] Institute for Materials Research, School of Process, Environmental and Materials Engineering, University of Leeds, Leeds, LS2 9JT, UK

[3] SuperSTEM Laboratory, STFC Daresbury Campus, Warrington WA4 4AD, UK

[4] Department of Materials, University of Oxford, Parks Road, Oxford OX1 3PH, UK

*Email: y.chao@uea.ac.uk

ABSTRACT

Silicon nanoparticles (SiNPs) can be synthesized by a variety of methods. In many cases these routines are non-scalable with low product yields or employ toxic reagents. One way to overcome these drawbacks is to use one-pot synthesis based on the chemical reduction of micelles. In the following study trichloroalkylsilanes of differing chain lengths were used as a surfactant, and the level of capping, surface bonding and size of the nanoparticles formed has been investigated. FTIR results show that the degree of alkyl capping for SiNPs with different capping layers was constant, although SiNPs bound with shorter chains display a much higher level of Si-O owing to the reaction of the ethanol used in the method with uncapped sites on the particle. SiNPs with longer chain length capping show a sharp Si-H peak on the FTIR, these were heated at reflux with the corresponding 1-alkene to fully cap these particles, resulting in a reduction/disappearance of this peak with a minimal change in the intensity of the Si-O peak. Other techniques used to analyze the surface bonding and composition, XPS, ^{1}H-NMR, and EDX, show that alkyl capped SiNPs have been produced using this method. The optical properties showed no significant change between the different capped SiNPs.

Keywords: silicon; nanoparticles; FTIR; XPS; quantum yield; HRTEM

Introduction

Silicon is used as a primary building block in semiconductor electronics and as a result is widely available, and relatively cheap (Boukai et al., 2008, Hochbaum et al., 2008). Other advantages of silicon include its low toxicity and low environmental impact (Boukai et al., 2008, Hochbaum et al., 2008). These are major factors which have helped drive interest in the synthesis and application of SiNPs over the past twenty years (Ahire et al., 2012, Wilson et al., 1993, Kang et al., 2011, Chao et al., 2007). Quantum confinement effects give SiNPs interesting optical, electronic and mechanical properties (Reboredo and Galli, 2005, Pavesi et al., 2000, Chao et al., 2006, O'Farrell et al., 2006, Rosso-Vasic et al., 2008). These are responsible for their wide range of potential applications including use in electrical devices, photovoltaic applications and bioimaging (Moore et al., 2011, Alsharif et al., 2009, Nishiguchi and Oda, 2002, Ostraat et al., 2001, Wang et al., 2011b, Warner et al., 2005a, Wang et al., 2012).

Currently, one of the most effective methods of synthesis of SiNPs uses electrochemical etching to produce H-terminated porous silicon which is then broken into nanoscale clusters and their surfaces capped using a suitable method, such as hydrosilylation (Kelly et al., 2011). The resulting SiNPs are of high purity with limited surface oxidation. However a major hindrance is the use of HF in the initial etching step, which is corrosive and highly toxic. Owing to this drawback, recent developments in the synthesis of SiNPs are moving away from electrochemical etching, and more towards chemical and physiochemical based methods such as inverse micelle and plasma synthesis (Wilcoxon et al., 1999, Mangolini et al., 2005, Neiner et al., 2006).

2

Early methods made use of surfactants, such as tetraoctylammonium bromide in toluene, to form inverse micelles, within which seeds of SiCl4 are formed (Warner et al., 2005b, Wilcoxon and Samara, 1999). The SiCl4 is reduced using a strong reducing agent such as LiAlH4. This reduces Si-Cl bonds within the seed to Si-Si and further reduces the Si-Cl bonds at the seed surface to Si-H, thus forming hydrogen capped SiNPs (Warner et al., 2005b, Wilcoxon and Samara, 1999). These are capped by a suitable capping method, such as palladium catalyzed hydrosilylation, and the surfactant removed (Warner et al., 2005b, Wilcoxon and Samara, 1999). However, the removal of surfactant is not a trivial task and due to the surfactant and the byproducts of such methods the particles produced are not as pure in comparison to other methods, such as the aforementioned electrochemical etching. The development of inverse micelle based methods is appealing because of the general monodispersity obtained, the potential of the use of these types of methods for size control and the fact that these experiments can be performed at room temperature and pressure.

In early 2011 a one-pot method was developed by Wang and co-workers that used trichloro(hexyl)silane as a surfactant which, on reduction, formed the SiNP capping layer (Wang et al., 2011a). This method results in a much higher yield over other inverse micelle syntheses as no surfactant removal is required, limiting loss of product. However, the resulting SiNPs show an increased proportion of oxide species, against SiNPs formed through electrochemical methods, which is attributed to incomplete capping of the SiNPs surface followed by oxidation of Si-H (Wang et al., 2011a).

In this study, a number of different ligands (hexyl, octyl, dodecyl and octadecyl)

have been tested to develop a picture of how the results of this method vary as the carbon chain on the surfactant is altered (Scheme 1). The major points of this work are: the level of capping, surface bonding and the size of the particles produced. Additional steps have been introduced to this method accordingly, such that optimum capping is achieved for each different alkyl chain.
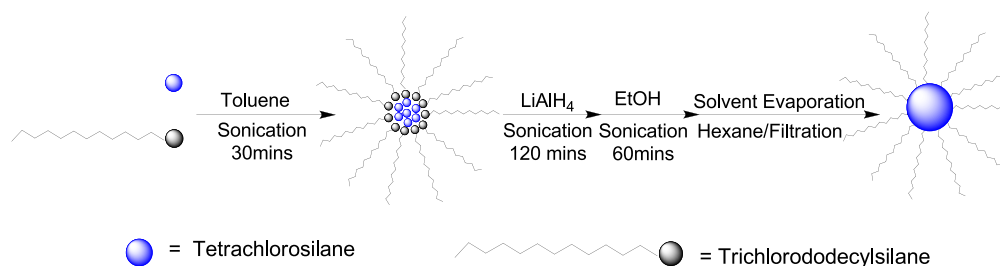
Scheme 1 Reaction scheme for the synthesis of SiNPs by the chemical reduction of micelles of tetrachlorosilane and trichloro(alkyl)silane surfactant

Experimental

Materials

Toluene (Fisher, 99.9 %) dried over sodium wire, ethanol (Sigma-Aldrich, 99.8 %) and hexane (Fisher. 99.9 %). Lithium aluminium hydride solution (Fisher, 1M in THF), silicontetrachloride (Sigma-Aldrich, 99 %), Trichloro(hexyl)silane (Sigma-Aldrich, 97 %), Trichloro(dodecyl)silane (Sigma-Aldrich, 95 %), Trichloro(octyl)silane (Sigma, 97 %), Trichloro(octadecyl)silane (Sigma, 90 %) all stored under nitrogen.

Synthesis of alkyl-capped SiNPs

Dry toluene (50 ml) was degassed by ten repetitions of 1 minute sonication under vacuum. To this an alkyl-SiCl3 based surfactant (0.7 mmol) and SiCl4 (0.1 mL, 0.7 mmol) were introduced and dispersed by vigorous shaking for 1 min followed by sonication for 30 mins. This was then reduced using a 1M LiAlH4

solution in THF (4 mL, 4 mmol) which was added dropwise over 5 minutes and ultrasonicated for 120 minutes. Ethanol (40 mL) was introduced to the reaction mixture, followed by ultrasonication for 60 minutes. All solvent was removed to give a white powder, which contained a mixture of byproduct and SiNPs. This was dissolved in hexane, filtered out using a PVDF syringe filter (450 nm) and dried *in vacuo* to give a clear pale yellow oil (~120 mg).

The dodecyl and octadecyl capped SiNPs were subjected to a further functionalisation step. The functionalised SiNPs were ultrasonicated for 5 minutes in a 0.04 M solution of the corresponding 1-alkene in toluene (10 ml). This mixture was heated under reflux conditions for 5 hours and dried to give dodecyl and octadecyl capped SiNPs as clear pale yellow oil.(Lie et al., 2002)

The samples have been analyzed using FTIR spectroscopy, X-ray photoemission spectroscopy (XPS), ^{1}H-NMR spectroscopy, UV/vis absorption spectroscopy, photoluminescence (PL) spectroscopy, Energy-dispersive X-ray spectroscopy (EDX), transmission electron microscopy (TEM), high resolution transmission electron microscopy (HRTEM), and aberration corrected scanning transmission electron microscopy (STEM).

FTIR spectroscopy

FTIR spectra were collected using a Perkin-Elmer Spectrum 100 ATR FTIR spectrometer. The gelatinous sample was placed on the crystal to take the measurement and the background was corrected by taking a spectrum of the clean crystal.

XPS measurement

XPS measurements were taken using a SCIENTA SES200 electron energy analyzer at beamline D1011 (MAXLab, Lund, Sweden). A few drops of a suspension of SiNPs in dichloromethane were cast onto a clean gold substrate. This was transferred immediately into a load-lock attached to ultra high vacuum (UHV) chamber. The typical base pressure of this chamber was maintained at approximately 1×10^{-9} mbar. For all photoemission spectra, the binding energies (BEs) are referred to the Au $4f_{7/2}$ line as measured on a gold foil in direct electrical contact with the sample, which lies at a BE of 84 eV.

^{1}H-NMR spectroscopy

^{1}H-NMR measurement of the samples dissolved in $CDCl_3$ were taken using a Varian 400 MHz NMR spectrometer. These samples were measured relative to chloroform from the lock solvent ($CDCl_3$).

UV/Vis absorption spectroscopy, photoluminescence and quantum yield

The UV/vis absorption spectra for samples dissolved in hexane in a quartz cuvette (10 mm × 10 mm) were taken with a Perkin-Elmer 35 UV/Vis double-beam spectrophotometer. The scan range was 200-700 nm at a rate of 900 nm·min^{-1}. The background was corrected by subtracting the spectrum for the blank solvent.

The photoluminescence (PL) spectra were taken for samples dissolved in hexane, in a quartz cuvette (10 mm × 10 mm), using a Perkin-Elmer LS55

spectrophotometer with emission slit width of 5 nm. The excitation wavelength was set at 280 nm.

The quantum yield (QY) was calculated with equation (1), by preparing solutions of the sample at varying concentrations in hexane, and measuring the absorbance at 340 nm and the area under the emission peak for each concentration. Only samples with an absorbance between 0.1 and 0.01 were used. The absorbance was plotted against the area and compared to a reference of known quantum yield (quinine sulphate, 54.6 % at 340 nm excitation). The reference was prepared in 1M H_2SO_4 solution at different concentrations and the procedure repeated as above. The gradient of both the sample and the reference were used in the following equation to give the quantum yield of the sample.

$$Q = Q_R \left(\frac{Grad}{Grad_R}\right)\left(\frac{\eta^2}{\eta_R^2}\right) \qquad (1)$$

where Q is the quantum yield of SiNPs, Q_R is the quantum yield of the reference fluorophore of known quantum yield, η is refractive index of sample, η_R is refractive index of reference. Grad is the gradient from a plot of integrated fluorescence intensity against absorbance. The refractive indicies used were those of the pure solvent.

HRTEM and TEM imaging

HRTEM studies were performed with a Philips CM200 FEGTEM microscope. Atomic number contrast (Z-contrast) STEM imaging was performed on a Nion UltraSTEM 100, operated at 100 kV using a cold field emission electron source, and a corrector capable of neutralizing aberrations up to fifth order. TEM samples were prepared by dropcast SiNPs solution onto graphene substrate. The

7

solvent was evaporated and TEM micrographs were typically taken at different spots of each grid. Samples were baked at 135 ^{o}C for approximately 7 hours in a turbo backed vacuum oven prior to STEM imaging to reduce contamination.

Results & Discussion

FTIR analysis suggests that capped SiNPs are formed, see Figure 1(a-d). This is determined by presence of Si-C peaks at approximately 1464 and 1260 cm^{-1} and C-H peaks at approximately 2922 and 2852 (Lie et al., 2002, Sato and Swihart, 2006). Other peaks observed in these spectra are Si-H peak at 2148 cm^{-1} and Si-O peaks at 1094 and 1018 cm^{-1} (Lie et al., 2002). The Si-O peaks cannot be distinguished in the longer chain alkyl capped SiNPs and show as a broad peak, see Figure 1 c) and d).

Comparison of FTIR spectra from each sample (Figure 1) shows that, relative to that of the Si-C bending vibrational peak at 1464 cm^{-1}, the intensity of the Si-O peaks is less for the samples produced using longer chained surfactants. The relative intensity of this peak is equivalent to that observed for alkyl capped SiNPs synthesized by electrochemical etching (Lie et al., 2002). These results also show that the relative intensity of the Si-H peak is greaterfor the SiNPs capped with longer alkyl chains. This suggests that when using a longer chain length of surfactant (R=12, 18) the level of oxidation is lower than when using a short chain length (R=6, 8).
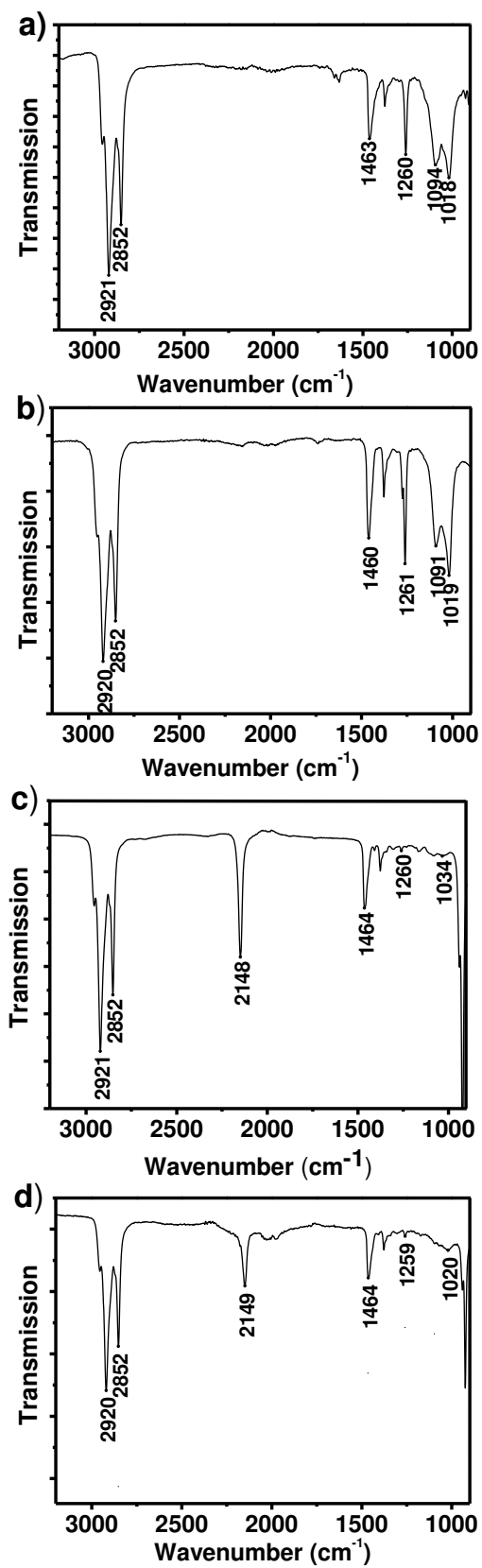
Figure 1 FTIR spectrum for each of a) hexyl-, b) octyl-, c) dodecyl- and d) octadecyl-capped
SiNPs.

Initial analysis of the product of this method attributed the high oxide levels observed in the hexyl capped SiNPs to the Si-H bonds undergoing oxidation with long term exposure to air (Wang et al., 2011a). The FTIR spectra were taken immediately after drying so there has been minimal exposure to air and in addition FTIR aging of another partially passified SiNP (dodecyl) shows no significant oxidation of the Si-H functionalities after 1 week (see supplementary information). However we observe rapid oxidation in the octyl and hexyl samples. It has been shown that the introduction of a protic solvent such as water or a primary alcohol can lead to oxidation by the solvent. The quenching step of LiAlH$_4$ introduced ethanol in to the reaction flask prior to exposure to air. Previous FTIR data of alkoxy SiNPs show a relatively sharp Si-O-C peak, observed at 1091cm^{-1}, rather than the typically broad Si-O peak observed in most alkyl capped SiNPs (Shirahata et al., 2009, Holmes et al., 2001, Pettigrew et al., 2003). The spectra for the alkoxy SiNPs have similar-shaped oxide profiles as those for both the hexyl- and octyl-capped SiNPs. This suggests that the higher oxide observed in these two samples is a result of the reaction of ethanol with the exposed Si-H surface, which would be as a result of incomplete surface capping. This reaction can occur at room temperature when stirred vigorously (Holmes et al., 2001). The longer chain capping layers act as a steric barrier to the ethanol preventing reaction with the Si-H sites and thus lower Si-O levels observed.

The alkoxy capping can be observed in ^{1}H-NMR spectra of samples displaying high oxide levels. On the ^{1}H-NMR of the octyl-capped SiNPs a small quartet can be observed at 3.66 ppm representing the CH$_2$ protons and a small broadened triplet 1.32 ppm which represents the CH$_3$ protons on the ethoxy capping (Figure

3). These features are absent from the NMR spectrum of the dodecyl-capped SiNPs, which is included in the supplementary information. The ^{1}H-NMR also supports the alkyl capping of SiNPs. This spectrum shows three proton environments, one at 0.55 ppm which is characteristic of a CH_2 attached to a silicon, as it is shifted upfeild from the other CH_2 protons which are shown at 1.18 ppm, and the CH_3 peak is observed at 0.78 ppm. These peaks show the same positioning as would be expected for the equivalent alkylsilane, but the sharp peak observed at 3.4 ppm with alkylsilane attributed to Si-H is absent.
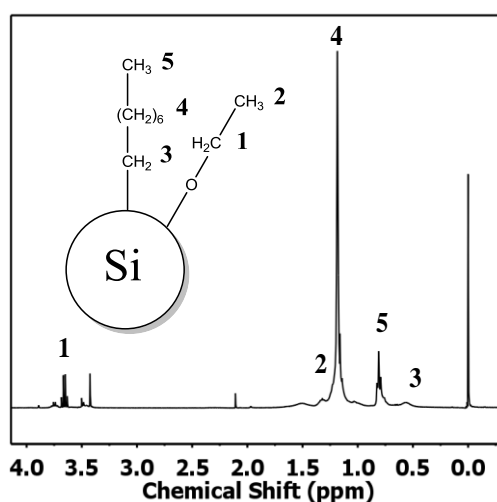
Figure 2 ^{1}H-NMR spectrum obtained from octyl-capped SiNPs dissolved in $CDCl_3$

An extra capping step was used as a result of the higher levels of Si-H observed in the FTIR. The FTIR spectra obtained from these samples after further reflux with corresponding 1-alkene are shown in Figure 3a) & b), and show a small increase in the relative intensity of the Si-O peaks, but a significant reduction in the intensity of the observed Si-H peak at 2125 cm^{-1}.

The increase in oxide levels after the reflux step can not be attributed to ethoxy capping due to the absence of ethanol and the shape of the peak, but the increased temperature and the presence of gases and contaminants in the

11

reagents and solvents (e.g. water) would lead to furtheroxidation thus explaining the results observed.
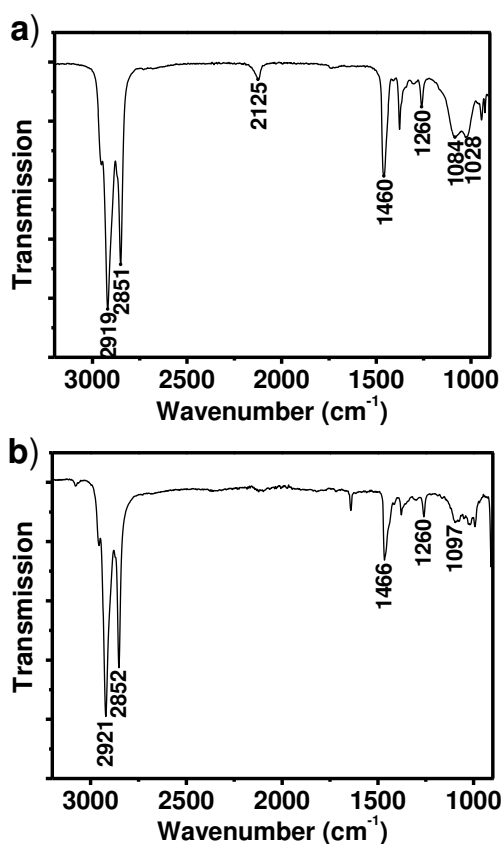
Figure 3 FTIR spectrum for each of a) dodecyl-, b) octdecyl-capped SiNPs obtained after additional reflux with corresponding 1-alkene

XPS measurements upon films of the samples made by the above method show resonance peaks for the elements expected within the material (Si, C and O) and a high level of capping. In Figure 4a), the Si2p spectrum for dodecyl-capped SiNPs is fitted with three components: at 99.92 eV, 102.93 eV, and 103.93 eV representing contributions from Si-Si, Si-C and Si-O respectively (Chao et al., 2011, Coxon et al., 2011). The percentage makeup from each is listed in the figure. The peak at 99.92 eV representing the Si-Si bonding within the center of the nanoparticles contributes 14.2 % of the total spectrum area within the fitted

12

energy window. The remaining 85.8 % is from Si-C and Si-O at the particle surface. Of this remainder 63.8 % is from Si-C and 22 % is Si-O meaning an estimated 75 % of the available surface has undergone alkyl capping. This compares favourably with H-terminated Si(111) surfaces bound by organic monolayers where 50 % surface coverage is typical (Sieval et al., 2001, Wallart et al., 2005). In Figure 4b), the C1s spectrum for dodecyl-capped SiNPs is fitted with two components: C-C at 285.18 eV and Si-C at 286.68 eV. 91.8 % of the spectrum area is from C-C within the carbon chains and the remaining 8.2% is made up by the Si-C where the passivating layer is bound to the silicon center. The ratio of the area of the spectrum represented by each component is close to 1:11, which is the exact ratio of Si-C to C-C bonds in the capped SiNPs.
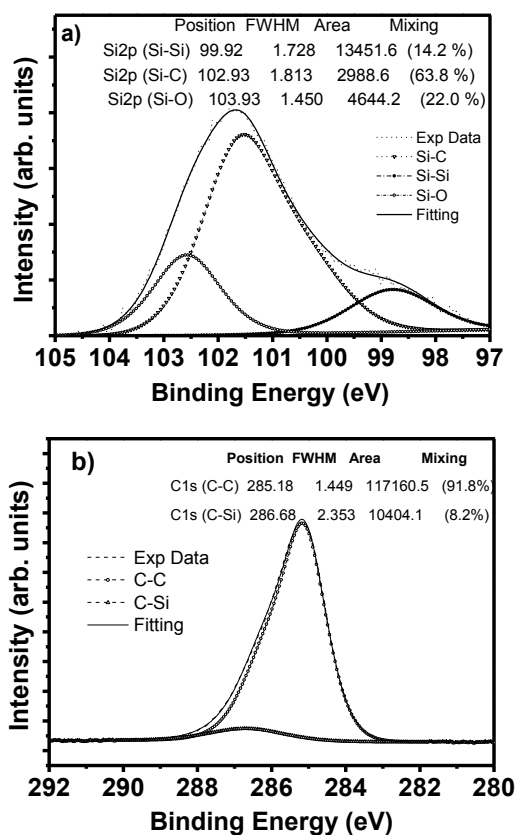
Figure 4 XPS spectra obtained from dodecyl capped SiNPs: a) Si2p and b) C1s. Both photoelectron spectra were collected with an incident photon energy of 630 eV

13

Figure 5 shows room temperature PL, UV/Vis spectra (Figure 5a), and quantum

yield measurement. The integrated emission intensity for the dodecyl-capped

SiNPs versus the corresponding UV/Vis absorbance at the same excitation

wavelength is plotted in Figure 5b. Shown alongside is the PL emission intensity

for the quinine sulfate reference. The quantum yield calculation (see

supplementary information) gives a value of 14 % at room temperature from the

ratio of the gradients of the linear fits to quinine sulfate and SiNPs, and the

known quantum yield of quinine sulfate (54.6%) at 340 nm, as reported

previously, where typical values for SiNPs lie between 4 % and 25 % (Wang et al.,

2011a, Wang et al., 2011b, Dickinson et al., 2008).
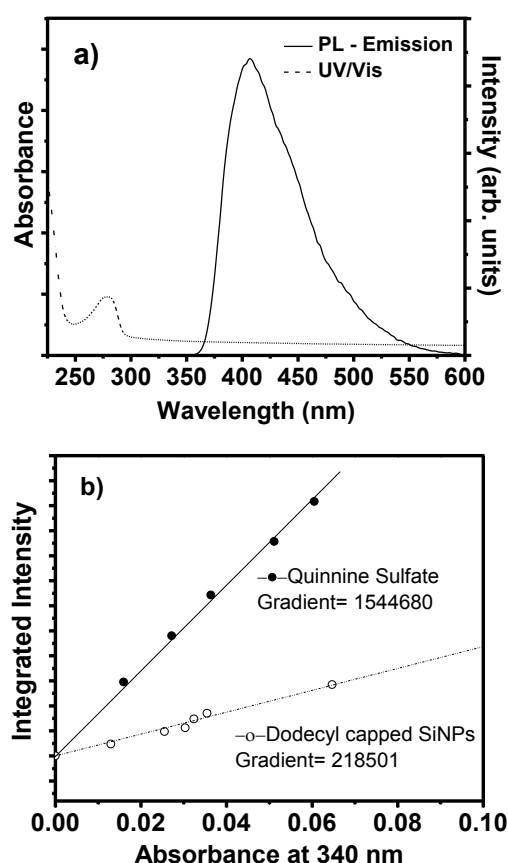
Figure 5 Room temperature photoluminescence and UV/Vis absorption spectra of dodecyl capped
SiNPS in hexane a); integrated photoluminescence intensity against absorbance for diluted
dodecyl-capped SiNPs in hexane and quinine sulphate in 1M H_2SO_4 solution b). Both were
collected under identical excitation conditions

Interestingly, the differences in capping layer did not greatly affect the optical properties or the size of the SiNPs. Each sample shows an identical UV/vis absorption peak at 280 nm and in each case the PL emission spectrum shows emission in the blue region at a wavelength of between 400 and 407 nm under excitation of 280 nm, Figure 5a). This shows there are no significant changes in optical properties between the differing lengths of the capping layers used.
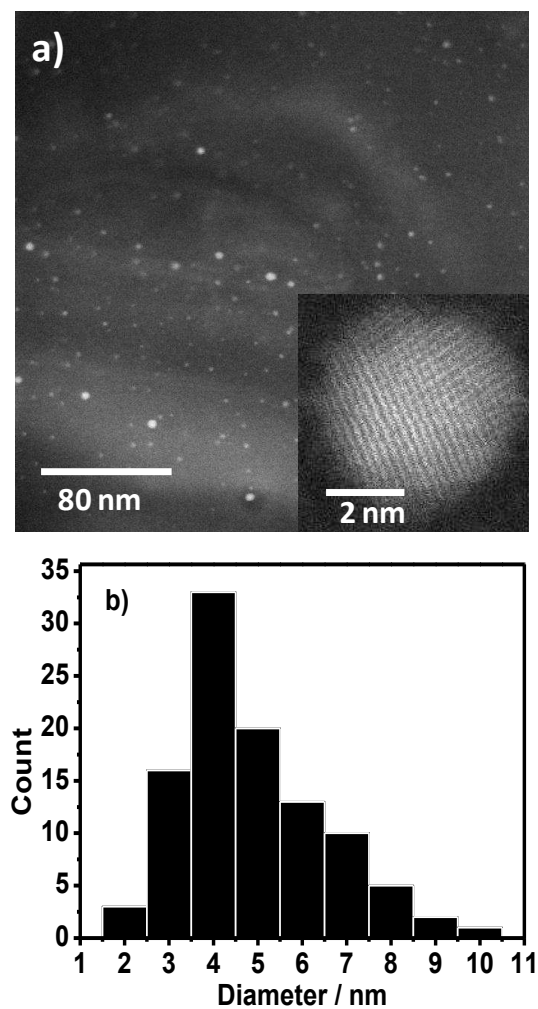
Figure 6 a) STEM image showing the distribution of sizes of hexyl capped SiNPs obtained from the reduction of hexyltrichorosilane/$SiCl_4$ micelles, inset: high resolution Z-contrast STEM image of an individual SiNPs showing it to be crystalline, b) histogram showing size distribution of alkyl-capped SiNPs.

TEM and STEM images show a similar distribution of sizes for all the samples produced. A Z-contrast STEM image showing the distribution of sizes of hexyl capped SiNPs obtained from the reduction of hexyltrichorosilane/$SiCl_4$ micelles is displayed in Figure 6a). Figure 6b) contains a histogram showing the size distribution of all the particles produced, and the mean diameters and standard deviations for each type of capping are shown in Table 1. The particles vary in size from 2.0 nm to 10 nm, with a peak number of counts at 4 nm in particle diameter. The mean diameter differs for each capping agent (surfactant) used and for hexyl, octyl and dodecyl shows a pattern of increasing mean size with increasing chainlength. However, the octadecyl surfactant breaks this pattern. It is to be expected that the surfactant will affect the size as shown in the results, but the way in which the increase of alkyl chain affects size requires further study, since these results do not show a definitive pattern. In addition, high resolution STEM imaging show that the particles are crystalline in nature, while EDX analysis confirms that the particles are silicon-rich (supplementary material). A Z-contrast STEM image showing the lattice fringes is shown in the inset of Figure 6a). The measured lattice fringe spacing in these crystalline particles is 0.31 nm, corresponding to the (111) interplanar spacing of the diamond cubic structure of silicon.

Table 1 The mean diameter and standard deviation of SiNPs from a sample of 100 particles

Capping	Mean diameter (nm)	Standard deviation (nm)
Hexyl	6.05	1.62
Octyl	6.31	1.61
Dodecyl	6.47	1.94
Octadecyl	6.21	1.71

The origin of the photoluminescence observed in Figure 5a) is complicated by the combination of both indirect and direct band gap transitions present in SiNPs (Holmes et al., 2001). However, there is strong theoretical evidence suggesting that 1-2 nm SiNPs with a hydrogen or carbon-terminated surface have direct band gap optical transitions that lead to photoluminescence in the blue region (Zhou et al., 2003, Warner et al., 2005b).

Conclusions

To summarize, the one-pot synthesis of alkyl-capped SiNPs, is viable for a wide range of capping (surfactant) chain lengths. The level of alkyl capping, despite initial appearances, is broadly consistent for all capping layers, although those capped with shorter chain length surfactants show a raised level of Si-O. This is because the ethanol used in the synthetic method is able to react with the uncapped Si-H on the surface of the particle. We have shown that the silicon nanoparticles produced by this method are crystalline and capped with alkyl chains.

Acknowledgements

References

AHIRE, J., WANG, Q., COXON, P. R., MALHOTRA, G., BRYDSON, R. M. D., CHEN, R. & CHAO, Y. 2012. Highly luminescent and non-toxic amine-capped nanoparticles from porous silicon: synthesis and their use in biomedical imaging. ACS Appl. Mater. Interfaces 4**:** 3285-3292.

ALSHARIF, N. H., BERGER, C. E. M., VARANASI, S. S., CHAO, Y., HORROCKS, B. R. & DATTA, H. K. 2009. Alkyl-Capped Silicon Nanocrystals Lack Cytotoxicity and have Enhanced Intracellular Accumulation in Malignant Cells via Cholesterol-Dependent Endocytosis. Small 5**:** 221-228.

BOUKAI, A. I., BUNIMOVICH, Y., TAHIR-KHELI, J., YU, J. K., GODDARD, W. A. & HEATH, J. R. 2008. Silicon nanowires as efficient thermoelectric materials. Nature 451**:** 168-171.

CHAO, Y., HOULTON, A., HORROCKS, B. R., HUNT, M. R. C., POOLTON, N. R. J., YANG, J. & ŠILLER, L. 2006. Optical luminescence from alkyl-passivated Si nanocrystals under vacuum ultraviolet excitation: Origin and temperature dependence of the blue and orange emissions. Appl. Phys. Lett. 88**:** 263119.

CHAO, Y., ŠILLER, L., KRISHNAMURTHY, S., COXON, P. R., BANGERT, U., GASS, M., KJELDGAARD, L., PATOLEO, S. N., LIE, L. H., O'FARRELL, N., ALSOP, T. A., HOULTON, A. & HORROCKS, B. R. 2007. Evaporation and deposition of alkyl-capped silicon nanocrystals in ultrahigh vacuum. Nat. Nanotechnol. 2**:** 486-489.

CHAO, Y., WANG, Q., PIETZSCH, A., HENNIES, F. & NI, H. 2011. Soft X-ray induced oxidation on acrylic acid grafted luminescent silicon quantum dots in ultrahigh vacuum. Phys. Status Solidi A-Appl. Mat. 208**:** 2424-2429.

COXON, P. R., WANG, Q. & CHAO, Y. 2011. An abrupt switch between the two photoluminescence bands within alkylated silicon nanocrystals. J. Phys. D: Appl. Phys. 44**:** 495301.

DICKINSON, F. M., ALSOP, T. A., AL-SHARIF, N., BERGER, C. E. M., DATTA, H. K., SILLER, L., CHAO, Y., TUITE, E. M., HOULTON, A. & HORROCKS, B. R. 2008. Dispersions of alkyl-capped silicon nanocrystals in aqueous media: photoluminescence and ageing. Analyst 133**:** 1573-1580.

HOCHBAUM, A. I., CHEN, R. K., DELGADO, R. D., LIANG, W. J., GARNETT, E. C., NAJARIAN, M., MAJUMDAR, A. & YANG, P. D. 2008. Enhanced thermoelectric performance of rough silicon nanowires. Nature 451**:** 163-167.

HOLMES, J. D., ZIEGLER, K. J., DOTY, R. C., PELL, L. E., JOHNSTON, K. P. & KORGEL, B. A. 2001. Highly luminescent silicon nanocrystals with discrete optical transitions. J. Am. Chem. Soc. 123**:** 3743-3748.

KANG, Z., LIU, Y. & LEE, S.-T. 2011. Small-sized silicon nanoparticles: new nanolights and nanocatalysts. Nanoscale 3**:** 777-791.

KELLY, J. A., SHUKALIAK, A. M., FLEISCHAUER, M. D. & VEINOT, J. G. C. 2011. Size-dependent reactivity in hydrosilylation of silicon nanocrystals. J. Am. Chem. Soc. 133**:** 19015-6.

LIE, L. H., DUERDIN, M., TUITE, E. M., HOULTON, A. & HORROCKS, B. R. 2002. Preparation and characterisation of luminescent alkylated-silicon quantum dots. J. Electroanal. Chem. 538-539**:** 183-190.

MANGOLINI, L., THIMSEN, E. & KORTSHAGEN, U. 2005. High-yield plasma synthesis of luminescent silicon nanocrystals. Nano Lett. 5**:** 655-659.

MOORE, D., KRISHNAMURTHY, S., CHAO, Y., WANG, Q., BRABAZON, D. & MCNALLY, P. J. 2011. Characteristics of silicon nanocrystals for photovoltaic applications. Phys. Status Solidi A-Appl. Mat. 208**:** 604-607.

NEINER, D., CHIU, H. W. & KAUZLARICH, S. M. 2006. Low-temperature solution route to macroscopic amounts of hydrogen terminated silicon nanoparticles. J. Am. Chem. Soc. 128**:** 11016-11017.

NISHIGUCHI, K. & ODA, S. 2002. Ballistic transport in silicon vertical transistors. J. Appl. Phys. 92**:** 1399-1405.

O'FARRELL, N., HOULTON, A. & HORROCKS, B. R. 2006. Silicon nanoparticles: applications in cell biology and medicine. Int. J. Nanomed. 1**:** 451-472.

OSTRAAT, M. L., DE BLAUWE, J. W., GREEN, M. L., BELL, L. D., BRONGERSMA, M. L., CASPERSON, J., FLAGAN, R. C. & ATWATER, H. A. 2001. Synthesis and

characterization of aerosol silicon nanocrystal nonvolatile floating-gate memory devices. Appl. Phys. Lett. 79**:** 433-435.

PAVESI, L., DAL NEGRO, L., MAZZOLENI, C., FRANZO, G. & PRIOLO, F. 2000. Optical gain in silicon nanocrystals. Nature 408**:** 440-444.

PETTIGREW, K. A., LIU, Q., POWER, P. P. & KAUZLARICH, S. M. 2003. Solution synthesis of alkyl- and alkyl/alkoxy-capped silicon nanoparticles via oxidation of Mg2Si. Chem. Mater. 15**:** 4005-4011.

REBOREDO, F. A. & GALLI, G. 2005. Theory of alkyl-terminated silicon quantum dots. J. Phys. Chem. B 109**:** 1072-1078.

ROSSO-VASIC, M., SPRUIJT, E., VAN LAGEN, B., DE COLA, L. & ZUILHOF, H. 2008. Alkyl-Functionalized Oxide-Free Silicon Nanoparticles: Synthesis and Optical Properties. Small 4**:** 1835-1841.

SATO, S. & SWIHART, M. T. 2006. Propionic-Acid-Terminated Silicon Nanoparticles:‚Äâ Synthesis and Optical Characterization. Chem. Mater. 18**:** 4083-4088.

SHIRAHATA, N., FURUMI, S. & SAKKA, Y. 2009. Micro-emulsion synthesis of blue-luminescent silicon nanoparticles stabilized with alkoxy monolayers. J. Cryst. Growth 311**:** 634-637.

SIEVAL, A. B., VAN DEN HOUT, B., ZUILHOF, H. & SUDHOLTER, E. J. R. 2001. Molecular modeling of covalently attached alkyl monolayers an the hydrogen-terminated Si(111) surface. Langmuir 17**:** 2172-2181.

WALLART, X., DE VILLENEUVE, C. H. & ALLONGUE, P. 2005. Truly quantitative XPS characterization of organic monolayers on silicon: Study of alkyl and alkoxy monolayers on H-Si(111). J. Am. Chem. Soc. 127**:** 7871-7878.

WANG, J., SUN, S., PENG, F., CAO, L. & SUN, L. 2011a. Efficient one-pot synthesis of highly photoluminescent alkyl-functionalised silicon nanocrystals. Chem. Commun. 47**:** 4941-4943.

WANG, Q., BAO, Y., ZHANG, X., COXON, P. R., JAYASOORIYA, U. A. & CHAO, Y. 2012. Uptake and Toxicity Studies of Poly-Acrylic Acid Functionalized Silicon Nanoparticles in Cultured Mammalian Cells. Adv. Health. Mater. 1**:** 189-198.

WANG, Q., NI, H., PIETZSCH, A., HENNIES, F., BAO, Y. & CHAO, Y. 2011b. Synthesis of water-dispersible photoluminescent silicon nanoparticles and their use in biological fluorescent imaging. J. Nanopart. Res. 13**:** 405-413.

WARNER, J. H., HOSHINO, A., YAMAMOTO, K. & TILLEY, R. D. 2005a. The synthesis of silicon nanoparticles for biomedical applications. In: CARTWRIGHT, A. N. O. M. (ed.) Nanobiophotonics and Biomedical Applications II.

WARNER, J. H., HOSHINO, A., YAMAMOTO, K. & TILLEY, R. D. 2005b. Water-soluble photoluminescent silicon quantum dots. Angew. Chem. Int. Ed. 44**:** 4550-4554.

WILCOXON, J. P. & SAMARA, G. A. 1999. Tailorable, visible light emission from silicon nanocrystals. Appl. Phys. Lett. 74**:** 3164-3166.

WILCOXON, J. P., SAMARA, G. A. & PROVENCIO, P. N. 1999. Optical and electronic properties of Si nanoclusters synthesized in inverse micelles. Phys. Rev. B 60**:** 2704-2714.

WILSON, W. L., SZAJOWSKI, P. F. & BRUS, L. E. 1993. Quantum Confinement in Size-Selected, Surface-Oxidized Silicon Nanocrystals. Science 262**:** 1242-1244.

WINTERS, B. J., HOLM, J. & ROBERTS, J. T. 2011. Thermal processing and native oxidation of silicon nanoparticles. J. Nanopart. Res. 13**:** 5473-5484.

ZHOU, Z., BRUS, L. & FRIESNER, R. 2003. Electronic Structure and Luminescence of 1.1- and 1.4-nm Silicon Nanocrystals: Oxide Shell versus Hydrogen Passivation. Nano Lett. 3**:** 163-167.